

## Initial Corrosion Behavior of Carbon Steel in Simulated Marine-Industrial Atmospheric Environment (Postprint)

**Authors:** Guo Mingxiao, Pan Chen, Wang Zhenyao, Han Wei

**Date:** 2017-11-21T00:00:00+00:00

### Abstract

This study employs weight loss analysis, X-ray diffraction analysis, and scanning electron microscopy (SEM) testing methods to conduct an in-depth investigation into the initial corrosion process and mechanism of carbon steel Q235 in a simulated marine industrial atmospheric environment, with a particular focus on exploring the influence of the synergistic effect of different ratios of SO<sub>2</sub> and Cl<sup>-</sup> on the mechanism of initial corrosion behavior of carbon steel. The results demonstrate that the initial corrosion of carbon steel Q235 in the simulated marine industrial atmospheric environment exhibits a characteristic transformation from an acceleration process to a deceleration process, and the corrosion kinetics of the acceleration process still follows the power function law  $D=Atn$ ; after 24 h of corrosion, the corrosion products exhibit a double-layer structure, i.e., a loose outer layer and a relatively dense inner layer. The synergistic effect of SO<sub>2</sub> and Cl<sup>-</sup> accelerates the corrosion of carbon steel; however, variations in their ratio do not significantly affect the corrosion weight loss of carbon steel, nor do they alter the composition of the corrosion products. The presence of SO<sub>2</sub> promotes a transformation in the corrosion morphology of carbon steel from localized corrosion to uniform corrosion.

### Full Text

#### Preamble

#### A Study on the Initial Corrosion Behavior of Carbon Steel Exposed to a Simulated Coastal-Industrial Atmosphere

Guo Mingxiao<sup>1,2</sup>, Pan Chen<sup>1\*</sup>, Wang Zhenyao<sup>1</sup>, Han Wei<sup>1</sup>

<sup>1</sup> Environmental Corrosion Research Center, Institute of Metal Research, Chinese Academy of Sciences, Shenyang 110016, China

<sup>2</sup> School of Materials Science and Engineering, University of Science and Technology of China, Shenyang 110016, China

Correspondent: PAN Chen, associate professor, Tel: (024)23893544, E-mail: cpan@imr.ac.cn

### Abstract

The initial corrosion process and mechanism of Q235 carbon steel in a simulated coastal-industrial atmosphere were investigated using weight loss analysis, X-ray diffraction (XRD), scanning electron microscopy (SEM), and electrochemical testing, with particular emphasis on the synergistic effects of varying SO<sub>2</sub> and Cl<sub>2</sub> ratios on the early-stage corrosion behavior. The results demonstrate that the initial corrosion of Q235 carbon steel in this environment exhibits a transition from acceleration to deceleration, with the accelerated stage following a power-law kinetic relationship  $D=At^n$ . After 24 h of exposure, the corrosion product layer displays a bilayer structure consisting of a loose outer layer and a relatively dense inner layer. The synergistic effect of SO<sub>2</sub> and Cl<sub>2</sub> accelerates corrosion, though variations in their ratio exert minimal influence on weight loss and do not alter the composition of corrosion products. SO<sub>2</sub> promotes a more uniform corrosion morphology on carbon steel.

**Keywords:** carbon steel, atmospheric corrosion, synergism

---

## 1. Introduction

Carbon steel, as the most widely used structural material, finds extensive applications in transportation, resources and environmental engineering, energy and power generation, construction, and agriculture. In most service environments, carbon steel is inevitably exposed directly to the atmosphere, making it susceptible to atmospheric corrosion. Consequently, research on the atmospheric corrosion of carbon steel has long been a subject of considerable interest. Wang et al. conducted experimental studies on carbon steel corrosion during atmospheric exposure and summarized the climatic conditions and atmospheric corrosivity across various natural environments in China, revealing significant regional variations in corrosion rates due to differing climates. Numerous studies have highlighted that carbon steel corrosion in coastal-industrial atmospheres is particularly severe. With rapid industrial development in many southeastern coastal cities of China, SO<sub>2</sub> pollution has become increasingly serious, creating a coastal-industrial atmosphere containing both Cl<sub>2</sub> and SO<sub>2</sub>. Therefore, investigating the corrosion behavior of carbon steel in such environments is essential.

Current research on steel corrosion in atmospheric environments primarily focuses on long-term behavior. Kucera et al. performed 8-year exposure experiments in Sweden and Czechoslovakia, demonstrating that carbon steel corrosion rates in environments containing SO<sub>2</sub> pollutants and chlorides could be described by linear equations, with coefficients correlating to SO<sub>2</sub> deposition rates. Liang

and Hou conducted 16-year exposure studies at seven test sites across China, showing that long-term atmospheric corrosion of steel follows a power-law relationship. However, studies on the initial corrosion behavior of carbon steel in coastal-industrial atmospheres remain scarce. Since corrosion products formed during the early stages of atmospheric corrosion exhibit varying compositions and structures depending on the environment, which significantly influence subsequent corrosion behavior, investigating initial-stage corrosion is crucial for understanding the underlying mechanisms.

Furthermore, SO<sub>2</sub> and Cl<sub>2</sub> are recognized as the most important corrosive species affecting steel atmospheric corrosion. Cai et al. studied the effects of chlorides and sulfur pollutants on carbon steel atmospheric corrosion, finding that synergistic effects exist during the initial stage but diminish as corrosion progresses. Qu et al. investigated the influence of NaCl and low-concentration SO<sub>2</sub> on A3 steel atmospheric corrosion, demonstrating that synergism between them caused significantly greater weight loss than either species alone. In coastal-industrial atmospheric environments, the synergistic effect of SO<sub>2</sub> and Cl<sub>2</sub> markedly accelerates steel corrosion and reduces service life. However, the mechanism by which varying SO<sub>2</sub>-to-Cl<sub>2</sub> ratios influences this synergistic effect during the initial corrosion stage remains unclear and requires further detailed investigation.

In summary, this work employs laboratory accelerated simulation methods, including traditional weight loss analysis, SEM, XRD, and electrochemical testing, to systematically investigate the initial corrosion mechanism of carbon steel in a simulated coastal-industrial atmosphere and to explore the influence of different SO<sub>2</sub>-to-Cl<sub>2</sub> ratios on this behavior.

## 2. Experimental Methods

### 2.1 Materials and Sample Preparation

The experimental material was Q235 steel with the following chemical composition (wt.%): C 0.18, Si 0.25, Mn 0.5, S 0.018, P 0.016, and Fe balance. Samples for weight loss and rust layer analysis measured 50 mm × 25 mm × 2.5 mm. All specimens were ultrasonically cleaned in acetone to remove oil, dehydrated with alcohol, and stored in a desiccator. After 24 h, samples for weight loss analysis were weighed using an analytical balance with 0.001 g precision. Samples for electrochemical analysis measured 10 mm × 10 mm × 2.5 mm.

### 2.2 Laboratory Accelerated Simulation Testing

Accelerated corrosion tests were conducted using a C4-180Pro temperature-humidity chamber. Since HSO<sub>3</sub> better represents the transformation behavior and characteristics of SO<sub>2</sub> under thin electrolyte films during corrosion, NaHSO<sub>3</sub> and NaCl were employed to simulate atmospheric SO<sub>2</sub> and Cl<sub>2</sub>, respectively. The experimental procedure involved uniformly spreading the corrosive medium on sample surfaces using a micro-syringe, oven-drying, and then placing specimens in the test chamber for accelerated corrosion testing. The test followed

a “wet/dry” alternating cycle of 3 h, comprising 1 h of wet conditions (90% relative humidity, 30 °C) and 2 h of dry conditions (60% relative humidity, 30 °C), with salt deposition every 24 h.

To deepen understanding of the SO<sub>2</sub> and Cl synergistic effect and facilitate corrosion control under different environments, this work utilized indoor cyclic wet/dry accelerated corrosion testing. While maintaining a constant total molar amount of S and Cl, the ratio of NaHSO<sub>3</sub> to NaCl in the corrosive medium was varied to investigate the influence of different SO<sub>2</sub>-to-Cl ratios on the initial corrosion mechanism and to reveal the underlying synergistic mechanisms.

Two groups of accelerated corrosion tests were conducted:

**(1) Accelerated Test I: Simulating Initial Corrosion in Coastal-Industrial Atmosphere**

A mixed salt solution of 0.15 mol/L NaCl + 0.05 mol/L NaHSO<sub>3</sub> (deposition amount: 10 L/cm<sup>2</sup>, ratio 3:1) was applied to sample surfaces for cyclic wet/dry corrosion testing. Test durations were 24, 48, 72, 96, and 120 h. For each period, three parallel samples were removed for weight loss analysis, one for morphology analysis, and four for electrochemical testing.

**(2) Accelerated Test II: Influence of Different SO<sub>2</sub>-to-Cl Ratios**

Single NaCl (0.2 mol/L), single NaHSO<sub>3</sub> (0.2 mol/L), and mixed NaCl-NaHSO<sub>3</sub> solutions with different ratios (0.15 mol/L NaCl + 0.05 mol/L NaHSO<sub>3</sub>, 0.1 mol/L NaCl + 0.1 mol/L NaHSO<sub>3</sub>, 0.05 mol/L NaCl + 0.15 mol/L NaHSO<sub>3</sub>) corresponding to ratios of 3:1, 1:1, and 1:3 were applied. All tests lasted 120 h.

### 2.3 Corrosion Weight Loss Analysis

Samples were derusted using a solution of 500 mL HCl (38% concentrated) + 500 mL distilled water + 20 g hexamethylenetetramine. After derusting, specimens were rinsed with distilled water and alcohol, dried with a hair dryer, placed in a desiccator, and weighed after 24 h (precision: 0.001 g). Weight loss data for each period represent the average of three parallel samples.

### 2.4 Rust Layer Composition Analysis

Samples for rust layer analysis (50 mm × 25 mm × 2.5 mm) were cut into 10 mm × 10 mm × 2.5 mm pieces. Phase analysis was performed using a Rigaku-D/max-2500PC XRD system with Cu K radiation at 50 kV and 250 mA, scanning at 2°/min for qualitative analysis of corrosion products.

### 2.5 Rust Layer Morphology Analysis

Surface and cross-sectional morphologies were examined using an ESEM XL30 FEG scanning electron microscope. For cross-sectional analysis, samples were encapsulated in epoxy resin at room temperature, cured, ground sequentially with sandpaper from 600 to 2000 grit, polished with W2.5 diamond paste, cleaned with alcohol, dried with a hair dryer, and then observed under SEM.

## 2.6 Electrochemical Analysis

Electrochemical measurements were performed using a PARSTAT 2273 workstation with a standard three-electrode system: saturated calomel electrode (SCE) as reference, Pt electrode as counter, and the corroded sample as working electrode. All potentials reported are relative to SCE. The electrolyte was 0.1 mol/L Na SO solution prepared with analytical reagents and distilled water at room temperature. Potentiodynamic polarization curves were scanned at 0.33 mV/s. Before testing, the open-circuit potential was allowed to stabilize until its variation was less than 1 mV/min.

## 3. Results and Discussion

### 3.1 Initial Corrosion Behavior in Simulated Coastal-Industrial Atmosphere

**3.1.1 Corrosion Kinetics** Weight loss measurement is the most common method for evaluating atmospheric corrosion, typically expressed as weight loss per unit area or average corrosion depth. The corrosion depth of steel can be calculated using:

$$D = \frac{W_t}{\rho S} \times 10^4 \quad (1)$$

where  $D$  is corrosion depth (m),  $W$  is weight loss (g),  $\rho$  is the density of Q235 carbon steel (7.86 g/cm<sup>3</sup>), and  $S$  is the total sample area (cm<sup>2</sup>).

The average corrosion rate  $V$  can be calculated from the corrosion depth:

$$V_a = \frac{D}{t} \quad (2)$$

where  $t$  is corrosion time (h). Figure [Figure 1: see original paper] shows the variation in average corrosion rate of carbon steel in the simulated coastal-industrial atmosphere over time. The corrosion rate initially increases gradually, reaching a maximum at 96 h, then decreases significantly. Thus, the initial corrosion process of Q235 carbon steel in this environment comprises two stages: corrosion acceleration and deceleration, closely related to the evolution of corrosion products on the steel surface.

The long-term atmospheric corrosion kinetics of steel traditionally follow a power-law relationship:

$$D = At^n \quad (3)$$

where  $A$  and  $n$  are constants dependent on the material and environment. To verify whether this relationship applies to the initial accelerated corrosion stage

in marine-industrial atmospheres, the weight loss data for Q235 carbon steel during the first 96 h were fitted using Eq. (3), as shown in Figure [Figure 2: see original paper]. The correlation coefficient  $R^2$  (0.9998) approaching 1 indicates that the initial corrosion behavior still follows the power-law relationship. In this experiment,  $n = 1.3998 (>1)$ , suggesting that the rust layer formed during the initial stage provides no protection to the substrate, and the corrosion rate increases gradually with exposure time during the first 96 h.

**3.1.2 Rust Layer Composition** Figure [Figure 3: see original paper] presents XRD patterns of corrosion products formed on Q235 carbon steel after different exposure periods. After 24 h, the corrosion products consist mainly of  $\text{-FeOOH}$  and  $\text{-FeOOH}$ , with trace amounts of  $\text{FeSO} \cdot 2.5\text{H}_2\text{O}$ . During the initial corrosion stage,  $\text{-FeOOH}$  is the primary product, while  $\text{SO}_2$  promotes preferential formation of  $\text{-FeOOH}$ . At 48 h,  $\text{-FeOOH}$  appears, whose formation depends on the presence and concentration of  $\text{Cl}^-$ . At this stage, the surface  $\text{Cl}^-$  concentration reaches a critical level necessary for  $\text{-FeOOH}$  formation.  $\text{-FeOOH}$  exhibits strong reducibility, thereby accelerating the corrosion process. With further exposure, the composition and relative content of corrosion products remain essentially unchanged.  $\text{FeSO} \cdot 2.5\text{H}_2\text{O}$  is detected throughout the corrosion process. This ferrous sulfate salt increases the conductivity of the thin electrolyte film, promoting electrochemical reactions. According to the acid regeneration cycle mechanism,  $\text{FeSO}_4$  is oxidized by oxygen to  $\text{FeSO}_5$ , which then hydrolyzes and oxidizes to form iron oxyhydroxides and free sulfuric acid, further accelerating atmospheric corrosion.

**3.1.3 Rust Layer Morphology** Macroscopically, the corrosion product color gradually darkens with exposure time, transitioning from orange-yellow to reddish-brown and then dark brown, with uniform distribution across the sample surface. Figures [Figure 4: see original paper]a-e show surface morphologies of the rust layer at different corrosion stages. After 24 h, spherical corrosion products form a thin layer that allows easy access of corrosive media to the substrate. By 48 h, the surface coverage increases but contains numerous pores that cannot effectively prevent ingress of corrosive species. With prolonged exposure, the surface product density gradually improves.

Cross-sectional morphologies (Figures [Figure 5: see original paper]a-e) reveal that after 24 h, the rust layer is thin and porous with many transverse and longitudinal cracks, offering minimal protection. At 72 h, distinct layering appears: a loose, porous outer rust layer and a cracked but relatively dense inner layer, though the boundary is not sharp. With further exposure, both layers thicken and densify. By 120 h, the inner layer becomes dense and crack-free, effectively blocking oxygen and corrosive media penetration, leading to decreased corrosion rates.

**3.1.4 Electrochemical Analysis** Figures [Figure 6: see original paper] and [Figure 7: see original paper] show potentiodynamic polarization curves and

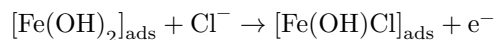
fitted corrosion current densities for rusted and blank samples in 0.1 mol/L Na<sub>2</sub>SO<sub>4</sub> solution. The blank sample's cathodic process is controlled by oxygen diffusion limiting current, while rusted samples exhibit significantly higher cathodic current densities due to reduction of corrosion products. From 24 to 72 h, the cathodic current density increases gradually, indicating that reduction of corrosion products becomes the dominant cathodic reaction. After 96 h, the cathodic current density stabilizes, likely due to stabilization of  $\alpha$ -FeOOH relative content in the rust layer. For the anodic process, rusted samples show higher current densities than blank samples due to both steel dissolution and oxidation of FeSO<sub>4</sub> corrosion products. Notably, the anodic current density decreases with exposure time, suggesting gradual inhibition of the anodic reaction. The fitted corrosion current densities (Figure [Figure 7: see original paper]) increase significantly from 24 to 72 h, then stabilize after 72 h, consistent with the weight loss results.

**3.1.5 Analysis of Initial Corrosion Evolution** In the simulated coastal-industrial atmosphere, Q235 carbon steel undergoes anodic dissolution of the substrate and cathodic reduction of dissolved oxygen under thin electrolyte films, forming a hydrolyzed Fe(OH)<sub>2</sub> layer. During drying, Fe(OH)<sub>2</sub> oxidizes to form various Fe oxides and hydroxides, partially transforming into  $\alpha$ -FeOOH and  $\beta$ -FeOOH, with SO<sub>2</sub> promoting preferential  $\alpha$ -FeOOH formation. At 48 h,  $\alpha$ -FeOOH appears as Cl<sup>-</sup> concentration reaches the critical level required for its formation. H<sub>2</sub>SO<sub>4</sub> in the simulated environment acidifies the thin electrolyte film, causing uniform chemical dissolution and gradual formation of FeSO<sub>4</sub> · 2.5H<sub>2</sub>O on the Q235 carbon steel surface. During the initial stage, the thin rust layer with its porous outer layer and cracked inner layer cannot effectively block corrosive media but instead prolongs surface wetting time, promoting rapid corrosion development. By 120 h, the thickened, densified rust layer with fewer cracks effectively blocks O<sub>2</sub> and corrosive media ingress, providing protection and reducing corrosion rates.

## 3.2 Influence of Different SO<sub>2</sub>-to-Cl Ratios

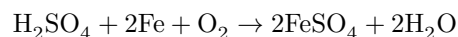
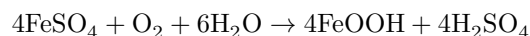
**3.2.1 Corrosion Weight Loss Analysis** Figure [Figure 8: see original paper] compares corrosion depths of Q235 carbon steel after 120 h exposure in different corrosive media. Corrosion loss in mixed SO<sub>2</sub>-Cl environments significantly exceeds that in single-medium environments, confirming synergistic acceleration of corrosion. The corrosive influence follows the order: NaHSO<sub>4</sub> + NaCl > NaHSO<sub>4</sub> > NaCl, with maximum weight loss occurring at a NaCl:NaHSO<sub>4</sub> ratio of 1:1.

Chloride ions, natural pollutants abundant in marine atmospheres, can penetrate rust layers to reach the substrate due to their small size, acting as catalysts in the corrosion reaction without being consumed. Cl<sup>-</sup> also increases electrolyte film conductivity and promotes microcell corrosion activity, causing partial dissolution of Fe(OH)<sub>2</sub> adsorbed on the Fe substrate:



These reactions may cause local dissolution of otherwise dense corrosion products, creating a porous outer rust layer and microcracks that facilitate transport of O<sub>2</sub> and corrosive media to the substrate.

SO<sub>2</sub> is recognized as the most corrosive atmospheric gas. In this study, H<sub>2</sub>SO<sub>4</sub> reacts with the substrate to form FeSO<sub>4</sub>, which gradually oxidizes to Fe<sub>2</sub>(SO<sub>4</sub>)<sub>3</sub>. Fe<sub>2</sub>(SO<sub>4</sub>)<sub>3</sub> then hydrolyzes and oxidizes to form iron oxyhydroxides and free sulfuric acid:



The regenerated FeSO<sub>4</sub> continues the cycle, allowing one SO<sub>2</sub> molecule to produce numerous iron rust molecules. The free acid generated during cycling dissolves unstable corrosion products, creating channels for O<sub>2</sub> and corrosive media ingress. This synergistic effect of local dissolution and acid regeneration results in significantly higher weight loss in mixed media than in single media. However, the synergistic effect does not intensify continuously with increasing SO<sub>2</sub> concentration. Maximum weight loss occurs at a 1:1 Cl<sup>-</sup>:SO<sub>2</sub> ratio because higher SO<sub>2</sub> concentrations generate more H<sub>2</sub>SO<sub>4</sub> through acid regeneration, accelerating corrosion. Yet when SO<sub>2</sub> concentration exceeds a critical value, it significantly promotes formation of FeOOH, a stable, continuous, and dense corrosion product that provides good protection, resulting in decreased weight loss. Nevertheless, variations in the SO<sub>2</sub>-to-Cl<sup>-</sup> ratio do not significantly affect weight loss or alter the composition of corrosion products, though SO<sub>2</sub> does promote more uniform corrosion morphology.

**3.2.2 Corrosion Product Composition Analysis** Figure [Figure 9: see original paper] shows XRD patterns of Q235 carbon steel after 120 h exposure in single NaCl, single NaHSO<sub>4</sub>, and various mixed media. The corrosion products in different mixed media consist mainly of FeOOH, Fe<sub>2</sub>(SO<sub>4</sub>)<sub>3</sub>, Fe<sub>2</sub>(SO<sub>4</sub>)<sub>3</sub>·2.5H<sub>2</sub>O, and FeSO<sub>4</sub>·2.5H<sub>2</sub>O, indicating that ratio variations do not change product composition. However, as the NaCl proportion decreases, FeOOH content decreases while Fe<sub>2</sub>(SO<sub>4</sub>)<sub>3</sub> content increases. The coexistence of FeOOH and FeSO<sub>4</sub>·2.5H<sub>2</sub>O accelerates corrosion, resulting in higher weight loss in mixed media. In single NaCl environments, corrosion products contain abundant FeOOH and minor Fe<sub>2</sub>(SO<sub>4</sub>)<sub>3</sub> due to high Cl<sup>-</sup> concentration promoting FeOOH formation.

In single NaHSO environments, products contain abundant  $\text{-FeOOH}$  and minor  $\text{-FeOOH}$ , confirming that  $\text{-FeOOH}$  preferentially forms in SO-containing environments.

**3.2.3 Corrosion Product Morphology Analysis** Cross-sectional morphologies after 120 h exposure (Figures [Figure 10: see original paper]a-e) show that in single NaCl environments, the rust layer is thin with large localized corrosion pits caused by pitting. In single NaHSO environments, the rust layer is similarly thin but without significant localized corrosion. In mixed NaCl-NaHSO environments, corrosion product thickness exceeds that in single media, consistent with weight loss results. Notably, a 3:1 NaCl:NaHSO ratio produces a distinct bilayer structure (porous outer layer and dense inner layer), while other ratios do not show clear layering. Since Cl causes local dissolution of corrosion products, higher Cl concentrations lead to more severe dissolution and porous outer layers, suggesting that layering is related to Cl concentration in the medium.

Surface morphologies after rust removal (Figures [Figure 11: see original paper]a-e) reveal that single NaCl exposure produces large, sparse corrosion pits, while mixed media exposure yields small, dense pits that become finer and more numerous as NaHSO proportion increases. Single NaHSO exposure results in uniform corrosion features. These observations confirm that SO promotes uniform corrosion morphology in environments containing both SO and Cl.

**3.2.4 Electrochemical Analysis** Potentiodynamic polarization curves after 120 h exposure (Figure [Figure 12: see original paper]) show that cathodic current density in single NaHSO is significantly lower than in single NaCl. This is attributed to the dominant corrosion product being  $\text{-FeOOH}$  in NaHSO versus  $\text{-FeOOH}$  in NaCl, with  $\text{-FeOOH}$  being less reducible. Although cathodic processes are suppressed in single NaHSO, anodic processes are enhanced due to FeSO oxidation in addition to steel dissolution, resulting in higher anodic current densities. Fitted corrosion current densities (Figure [Figure 13: see original paper]) show similar values across different mixed media, all significantly higher than in single media, with NaHSO alone producing higher current density than NaCl alone, consistent with weight loss results.

## 4. Conclusions

- (1) The initial corrosion rate of Q235 carbon steel in simulated coastal-industrial atmospheres first increases then decreases, with the accelerated stage following the power-law relationship  $D=At$ .
- (2) The presence of  $\text{-FeOOH}$  and FeSO corrosion products accelerates corrosion. After 24 h, a bilayer rust structure forms with a porous outer layer and relatively dense inner layer, with layering possibly related to Cl concentration in the medium.

- (3) The synergistic effect of SO<sub>2</sub> and Cl<sup>-</sup> accelerates carbon steel corrosion during the initial stage, but variations in their ratio do not significantly affect weight loss or alter corrosion product composition. SO<sub>2</sub> promotes a more uniform corrosion morphology.

## References

- [1] Yu Q C, Wang Z Y, Wang C. Corrosion behaviors of low alloy steel and carbon steel deposited with NaCl and NaHSO<sub>4</sub> under dry/humid alternative condition [J]. *Acta Metall. Sin.*, 2010, 46: 1133
- [2] Leygraf C, Graedel T. translated by Han E H, et al. *Atmospheric Corrosion* [M]. Beijing: Chemical Industry Press, 2005: 121
- [3] Wang Z Y, Yu G C, Han W. A survey of the atmospheric corrosiveness of natural environments in China [J]. *Corros. Prot.*, 2003, 24(8): 323
- [4] Wang S, Yang S, Gao K, et al. Corrosion behavior and corrosion products of a low-alloy weathering steel in Qingdao and Wanning [J]. *Int. J. Miner, Metall. Mater.*, 2009, 16(1): 58
- [5] Wan Y, Yan C W, Cao C N. Atmospheric corrosion of A3 steel deposited with different salts [J]. *Acta Phys. Chim. Sin.*, 2004, 20: 659
- [6] Ma Y, Li Y, Wang F. Corrosion of low carbon steel in atmospheric environments of different chloride content [J]. *Corros. Sci.*, 2009, 51: 997
- [7] Wang Z Y, Yuan Q C, Wang C, et al. Corrosion behaviors of steels in marine atmospheric environment with SO<sub>2</sub> pollution [J]. *Sci. Bull.*, 2012, 57: 2991
- [8] Kucera V, Knotkova D, Gullman J, et al. Corrosion of structural metals in atmospheres with different corrosivity at 8 year' s exposure in Sweden and Czechoslovakia [J]. *Key Eng. Mater.*, 1991, 20: 167
- [9] Liang C F, Hou W T. Sixteen-Year atmospheric corrosion exposure study of steels [J]. *J. Chin. Soc. Corros. Prot.*, 2005, 25: 1
- [10] Cai J P, Zheng Y P, Liu S R. Synergistic effect of chloride and sulphur-bearing pollutant in atmospheric corrosion of mild steel [J]. *J. Chin. Soc. Corros. Prot.*, 2009, 16: 303
- [11] Qu Q, Yan C W, Zhang L, et al. Synergism of NaCl and SO<sub>2</sub> in the initial atmospheric corrosion of A3 steel [J]. *Acta Metall. Sin.*, 2002, 38: 1062
- [12] Nishimura T, Katayama H, Noda K, et al. Electrochemical behavior of rust formed on carbon steel in a wet/dry environment containing chloride ions [J]. *Corrosion*, 2000, 56: 935
- [13] Lyon S B, Thompson G E, Johnson J B, et al. Accelerated atmospheric corrosion testing using a cyclic wet/dry exposure test: aluminum, galvanized steel, and steel [J]. *Corrosion*, 1987, 43: 719

- [14] Dunn D S, Bogart M B, Brossia C S, et al. Corrosion of iron under alternating wet and dry conditions [J]. *Corrosion*, 2000, 56: 1
- [15] Yamashita M, Konishi H, Kozakura T, et al. In situ observation of initial rust formation process on carbon steel under Na<sub>2</sub>SO<sub>4</sub> and NaCl solution films with wet/dry cycles using synchrotron radiation X-rays [J]. *Corros. Sci.*, 2005, 47: 2492
- [16] Antony H, Perrin S, Dillmann P, et al. Electrochemical study of indoor atmospheric corrosion layers formed on ancient iron artefacts [J]. *Electrochim. Acta*, 2007, 52: 7754
- [17] Hao L, Zhang S, Dong J, et al. Rusting evolution of MnCuP weathering steel submitted to simulated industrial atmospheric corrosion [J]. *Metall. Mater. Trans.*, 2012, 43A: 1724
- [18] Hao L. Rusting Evolution and Anti-corrosion Mechanism of MnCu-P/Mo Weathering Steels [D]. Shenyang: Institute of Metal Research, 2011
- [19] Li Q X, Wang Z Y, Han W, et al. Analysis on the corrosion rust of carbon steel exposed to Salt Lake area for 25 months [J]. *Acta Phys. Chim. Sin.*, 2008, 24: 1459
- [20] Tian Z Q, Wang C B, Kong X D, et al. Effect of rust layer on corrosion resistance of hull steel [J]. *Equip. Environ. Eng.*, 2012, 09(3): 66
- [21] Bai Y G, Tian N, Liu C M, et al. Study on the weather resistance and corrosion process of 09CuPTiRE steel [J]. *J. Mater. Metall.*, 2003, 2(1): 63
- [22] Hao L, Zhang S, Dong J, et al. A study of the evolution of rust on Mo-Cu-bearing fire-resistant steel submitted to simulated atmospheric corrosion [J]. *Corros. Sci.*, 2012, 54(1): 244
- [23] Svensson J E, Johansson L G. A laboratory study of the initial stages of the atmospheric corrosion of zinc in the presence of NaCl - Influence of SO<sub>2</sub> and NO [J]. *Corros. Sci.*, 1993, 24(34): 721
- [24] Xiao K, Dong C F, Li X G, et al. Effect of deposition of NaCl on the initial atmospheric corrosion of Q235 [J]. *J. Chin. Soc. Corros. Prot.*, 2009, 26: 26
- [25] Zhang X Y, Cai J P, Ma Y J, et al. Analysis on atmospheric corrosion of weathering and carbon steels [J]. *Corros. Sci. Prot. Technol.*, 2004, 16: 389
- [26] Mendoza A R, Corvo F. Outdoor and indoor atmospheric corrosion of carbon steel [J]. *Corros. Sci.*, 1999, 41(1): 75
- [27] Singh D D N, Yadav S, Saha J K. Role of climatic conditions on corrosion characteristics of structural steels [J]. *Corros. Sci.*, 2008, 50(1): 93
- [28] Dawson J L, Ferreira M G S. Crevice corrosion on 316 stainless steel in 3% sodium chloride solution [J]. *Corros. Sci.*, 1986, 26: 1

[29] Weissenrieder J, Leygraf C. In situ studies of filiform corrosion of iron [J]. J. Electrochem. Soc., 2004, 151: B165

[30] Wang J H, Wei F I, Chang Y S, et al. The corrosion mechanisms of carbon steel and weathering steel in SO<sub>2</sub> polluted atmospheres [J]. Mater. Chem. Phys., 1997, 47(1): 1

[31] Misawa T, Hashimoto K, Shimodaira S. The mechanism of formation of iron oxide and oxyhydroxides in aqueous solutions at room temperature [J]. Corros. Sci., 1974, 14: 131

[32] Evans U R, Taylor C A J. Mechanism of atmospheric rusting [J]. Corros. Sci., 1972, 12: 227

*Note: Figure translations are in progress. See original paper for figures.*

*Source: ChinaXiv –Machine translation. Verify with original.*